ARCHIVES OF ELECTRICAL ENGINEERING VOL. 67(4), pp. 845–855 (2018)

DOI 10.24425/aee.2018.124744

The effect of winding topologies on the performance of flux-switching permanent magnet machine having different number of rotor poles

CHUKWUEMEKA CHIJIOKE AWAH, OGBONNAYA INYA OKORO

Department of Electrical/Electronics Engineering, Michael Okpara University of Agriculture PMB 7267 Umudike, Nigeria
e-mails: awahchukwuemeka@gmail.com, profogbonnayaokoro@ieee.org

(Received: 13.06.2018, revised: 26.09.2018)

Abstract: Comparison of the electromagnetic performance of a flux-switching permanent magnet (PM) machine having two separate stators as well as different winding topologies is investigated in this paper. Different stator and rotor pole combinations of these machines are also considered. The analysis includes the open-circuit and on-load characteristics of the analyzed machines. It is observed that, the largest fundamental values of electromagnetic torque, for each winding topology, is seen in the 11-rotor-pole and 10-rotor-pole machines having alternate- and all-pole-wound configurations, respectively. Moreover, significant ripple is observed in the waveforms of the even-number rotor pole machines compared to their corresponding odd-number rotor pole counterparts. Overall, the alternate-pole-wound machines essentially have larger torque-density than their equivalent all-pole-wound ones. The investigated machine is also tested for validation.

Key words: average torque, copper loss, phase back-EMF, and winding topologies

1. Introduction

Permanent magnet (PM) machines, especially the flux-switching type have been researched extensively and yet tremendous research are still on-going in this area due to their abundant advantages such as high torque / power density, good thermal dissipation ability, better efficiency and reliability etc. [1] and [2], over other PM machines of the same size.

Although the machines with alternate-pole-wound topology exhibit higher output torque compared to their all-pole-wound counterparts, they are usually characterized by high magnetic stress and larger torque ripple, as well as higher harmonic contents relative to the all-pole-wound machines as demonstrated in [3]. More so, the alternate-pole machines have a larger amount of inductances compared to the all-pole-wound ones. Thus, this often leads to quicker saturation of their magnetic circuit/path. It is noted in [4] that, the higher inductance values of

the alternate-pole-wound machines are desirable qualities for fault-tolerance and extended speed range applications. Nevertheless, these alternate-pole-wound machines have significant amount of permanent magnet eddy current losses [5], owing to their high possession of magnetomotive force (MMF) sub-harmonic contents.

Further, the all-pole-wound machines have enhanced efficiency because they have a lower effect of armature reaction compared to other types of machine configurations [5] and [6]. Furthermore, a study in [6] shows that the all-pole-wound machines are capable of producing more sinusoidal back-EMF waveforms which are essential for control purposes, albeit with a lower winding factor which would also influence its fundamental back-EMF and electromagnetic torque potentials.

It is pointed out in [7] that, the alternate-pole-wound machines have lower machine performance compared to their all-pole-wound counterparts during post-fault mode, owing to their high MMF sub-harmonic characteristics. Similarly, the studies in [8] illustrate that the alternate-pole-wound machines have better thermal capability than their all-pole-wound counterparts due to its lower resistance, in addition to the higher amount of insulation materials needed to isolate the phases of the all-pole-wound machines. It is also noted in [8] that an open slot machine having all-pole-wound topology possesses a larger amount of torque ripple compared to alternate-pole-wound types. Furthermore, a comparative study of the winding layer effects on the overall performance of switched flux PM machines given in [9], shows that the torque capabilities of the machines reduce with an increasing number of winding layers due to the consequent effect of their various stack fill factors. However, the highest amount of undesirable features such as total harmonic distortion and losses are recorded in the alternate-pole-wound machines.

It is worth mentioning that, the overall performance of switched flux permanent magnet machines having a single stator configuration is greatly affected by its stator and rotor pole combinations as well as the adopted winding topology as detailed in [10]. Furthermore, it is proven in [11], that the electromagnetic performance of permanent magnet machines is significantly influenced by its winding factor characteristics. Thus, the higher the winding factor, the better its performance.

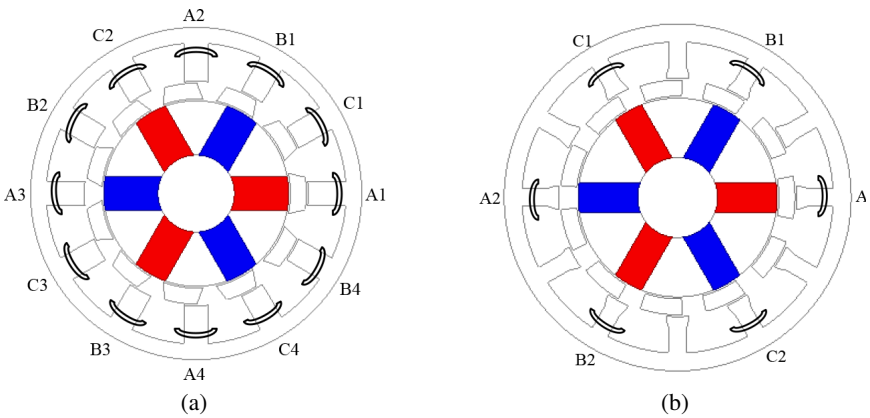

Fig. 1. Schematic diagram of the analyzed machine having different winding topology, 11-rotor: all-pole-wound (a); alternate-pole-wound (b)

It is also noted in [11], that the machines having a single-layer winding configuration have larger torque than their double-layer wound equivalents. Moreover, the quantitative comparison of permanent machines having different winding and stator structures presented in [12] shows that the machines having an odd number of rotor poles have lower loss and hence better efficiency than their corresponding machines with an even number of rotor poles. Similarly, the machines equipped with a single-layer winding topology is less efficient compared to its equivalent machine with a double-layer topology, owing to its high loss characteristics as stated in [12].

In this paper, a comparative analysis of the electromagnetic performance of flux-switching PM machines having different stators, as well as different winding topologies i.e. all- and alternate-pole-wound configurations is given. The schematic diagram of the developed double-stator PM machine having different winding topologies is displayed in Fig. 1. This work is subdivided into the following sections: Introduction, methodology, electromagnetic performance, experimental validation and conclusion.

2. Methodology

The developed machine has an outer diameter of 90 mm, 25 mm axial length, and 72 number of turns per phase. All the analysis is computed using a two-dimensional finite element analysis (2D-FEA) simulation tool. First, the investigated machines were optimized using the in-built genetic algorithm approach of the Ansoft-Maxwell FEA software with a goal for maximum torque, considering their geometric parameters such as the aspect ratio, back-iron thickness, PM thickness etc. Thereafter, the windings of the designed FEA model are supplied by a balanced three-phase (ABC) sinusoidal currents given in (1)–(3):

$$I_A = I_{\max} \sin(P_r \omega_r \cdot \text{time} + \phi_o), \tag{1}$$

$$I_B = I_{\max} \sin\left(P_r \omega_r \cdot \text{time} - \frac{2 \cdot pi}{3} + \phi_o\right), \tag{2}$$

$$I_C = I_{\max} \sin\left(P_r \omega_r \cdot \text{time} + \frac{2 \cdot pi}{3} + \phi_o\right), \tag{3}$$

where $I_{\max}$ is the maximum input current, P_r is the number of rotor poles, ω_r is the rotational speed, ϕ_o is initial current advance angle (which is zero in this study).

It is worth mentioning that, the rare earth permanent magnet material used in this paper is the Neodymium-Iron-Boron (Nd-Fe-B), which has a magnetic remanence of 1.2 T and a relative recoil permeability of 1.05. Further, the selected rotor and stator tooth numbers of the investigated machine are determined using (4).

$$\frac{P_s}{P_r} = \frac{2\phi_n b}{2\phi_n b \pm k}, \tag{4}$$

where ϕ_n is the number of stator phase windings, b and k are positive integers, P_s and P_r are the stator and rotor tooth numbers.

Also, the electrical frequency, f_e of the analyzed machines is directly related to its rotor tooth number as given in (5).

$$f_e = \frac{\omega_r P_r}{60}, \tag{5}$$

where ω_r is the rotor speed (rpm).

3. Electromagnetic performance

In the developed machine, the generated flux is being modulated by the rotor iron pieces. However, not all the flux reaches the windings in the outer stator because some flux returns back to the iron piece, which in other words also acts as a leakage path. This flux leakage effect could be seen from the 2D-FEA flux lines of Fig. 2; the flux leakage phenomenon is normal in magnetic gears and magnetically-geared machines [13, 14] and [15], and in turn influences the amount of transmitted torque since the output torque depends upon the modulated flux by the rotor iron pieces. This effect is not very common with other conventional permanent magnet machines, where a fringing effect is obtainable. The induced open-circuit phase electromotive force (EMF) of the investigated machines operated at 400 rpm is compared in Figs. 3 and 4, in addition to their resultant harmonic spectra.

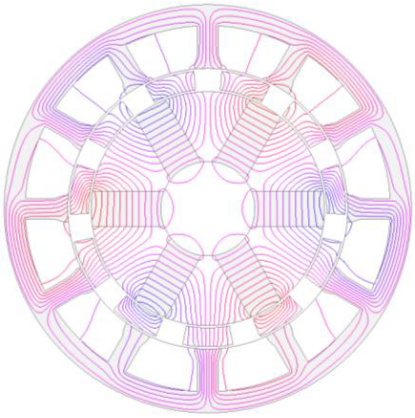

Fig. 2. The flux-lines distribution on no-load, 11-rotor pole

The induced electromotive force (EMF) of the analyzed machine is given in (6),

$$E = -N_t \Omega \frac{\mathrm{d}\,\Phi}{\mathrm{d}\,\theta}, \tag{6}$$

where N_t is the phase number of turns, Ω is the rotational angular velocity, Φ is the flux, θ is rotor angular position [16].

It should be noted that the alternate-pole-wound machines exhibit larger fundamental EMF amplitudes relative to their all-pole-wound equivalents. The results reveal that the even-rotor pole machines are characterized by even order harmonics, which is the origin of their asymmetric waveforms. It is also clear that the EMF waveforms of the 4-rotor pole machines are unbalanced and non-sinusoidal in both situations.

In order to obtain a balanced and symmetrical back-EMF waveform, then the conditions in (7) and (8) must be satisfied for the all-pole- and alternate-pole-wound topologies, respectively, as stated in [17].

$$\frac{P_s}{HCD(P_s, P_r)} = 6k, \tag{7}$$

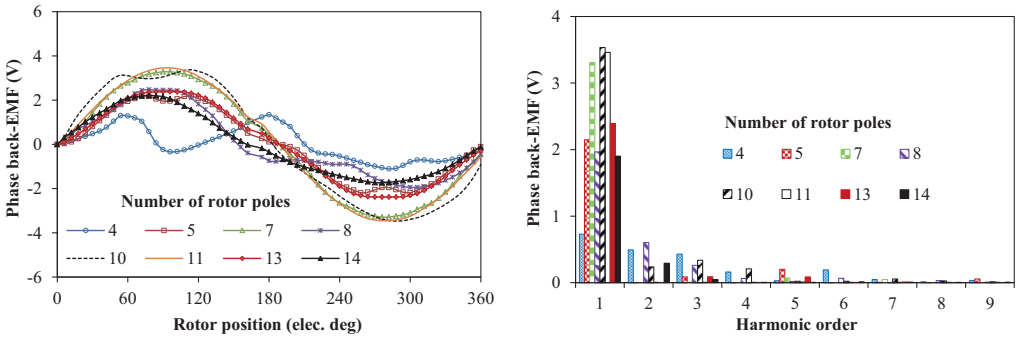

(a) Waveforms (b) Spectra

Fig. 3. Comparison of open-circuit phase back-EMF in the analysed machines having all-pole-wound, 400 rpm

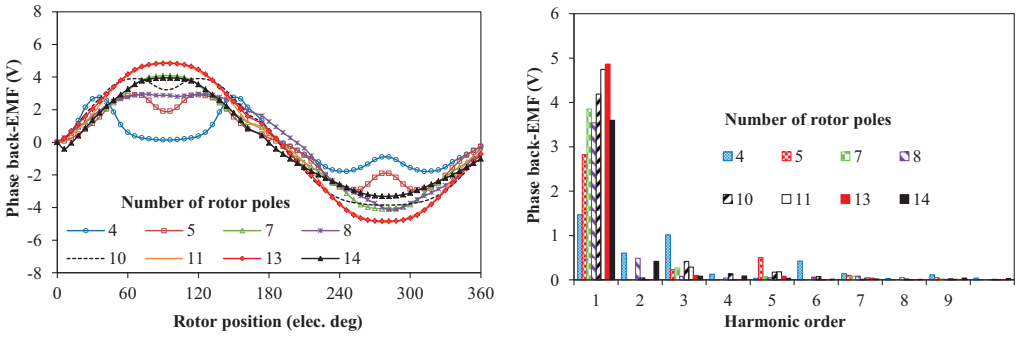

(a) Waveforms (b) Spectra

Fig. 4. Comparison of open-circuit phase back-EMF in the analysed machines having alternate-pole-wound, 400 rpm

$$\frac{P_s}{HCD(P_s, P_r)} = 12k, \tag{8}$$

where P_s and P_r are the stator and rotor tooth numbers, HCD is the highest common divisor, and k represents positive integer values [17].

The total output torque of any given permanent magnet machine could be estimated using (9). However, since the electromagnetic torque of flux-switching PM machines, to which the investigated machine belongs, is mainly contributed by the permanent magnet with a negligible reluctance torque component; therefore, the total output torque, T_o, of the compared machines is approximately expressed in (10).

$$T_o = T_{PM} + T_{rel} + T_c\,, \tag{9}$$

where: T_{PM}, T_{rel}, T_c are the magnetic torque, reluctance torque and cogging torque, respectively.

$$T_o = \left({}^{m}/_{2}\right) P_r \psi_{PM} N_t I_q + T_c\,, \tag{10}$$

where m is the number of phase(s), ψ_{PM} is the flux-linkage due to the magnets, N_t is the phase number of turns, I_q is the quadrature axis current, T_c is the cogging torque which results due to the interaction between the salient-pole structures and the permanent magnets.

The variation of the electromagnetic torque with a rotor position together with their respective spectra is depicted in Figs. 5 and 6. Moreover, the largest fundamental electromagnetic torque is obtained in the 10-rotor-pole and 11-rotor-pole machines having all- and alternate-pole-wound topologies, respectively.

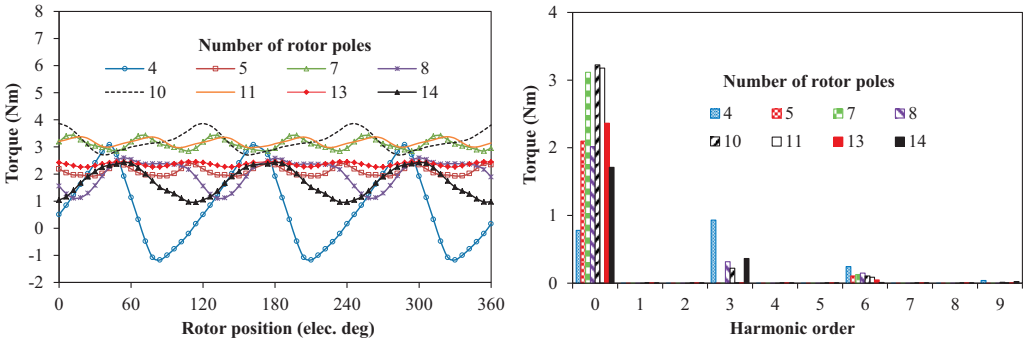

(a) Waveforms (b) Spectra

Fig. 5. Comparison of torque waveforms and spectra in all-pole-wound machines, at fixed copper loss

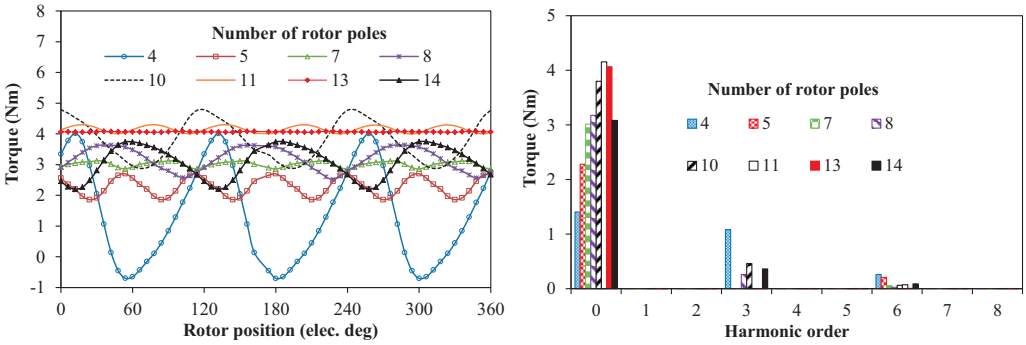

(a) Waveforms (b) Spectra

Fig. 6. Comparison of torque waveforms and spectra in alternate-pole-wound machines, at fixed copper loss

It is observed that, the torque ripple in even number rotor pole machines, especially the 4-rotor pole machine, is significantly larger than that of the compared odd rotor pole ones. This is as a result of their large harmonic contents. In particular, these sets of even numbers of rotor pole machines have dominant 3rd order harmonics as seen from the spectra of Figs. 5(b) and 6(b), unlike the odd rotor pole machines.

The saturation curves of the analysed machines are shown in Figs. 7 and 8 in terms of the torque variation with current and copper loss, respectively. It should be noted that, the 11-rotor-

pole machine exhibits the largest torque density under rated conditions compared to the other investigated machines, although the 10-pole machines could withstand heavy overload pressure than the rest of other machines, as seen from Figs. 7 and 8. The results also reveal that when the magnetic circuit is not severely saturated, the 10-pole and 11-pole machines have the largest torque density in the respective winding topologies, i.e. all- and alternate-pole-wound. The least amount of torque is seen in the 4-pole machines.

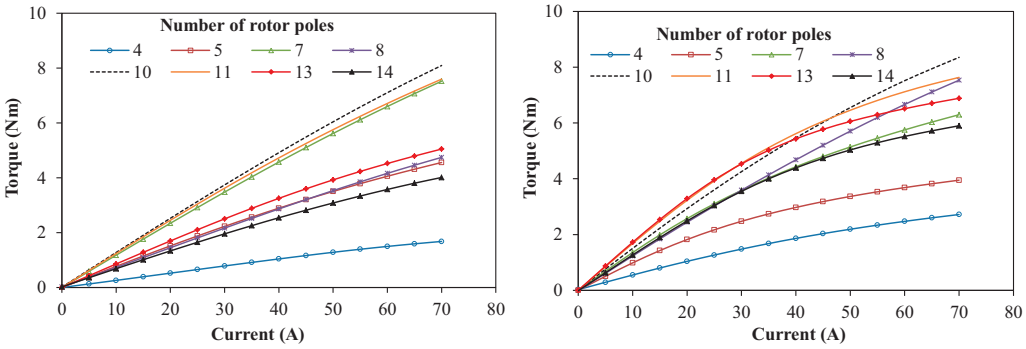

(a) All-pole-wound (b) Alternate-pole-wound

Fig. 7. Comparison of average torque against current, $i_d = 0$

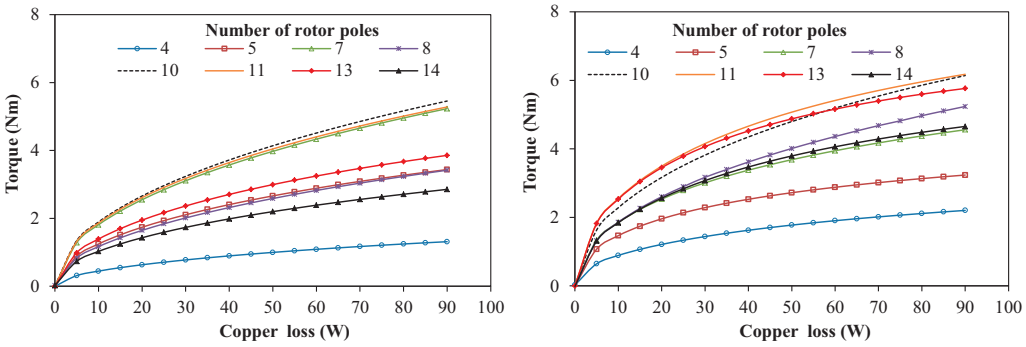

(a) All-pole-wound (b) Alternate-pole-wound

Fig. 8. Comparison of torque against copper loss, $i_d = 0$

The predicted losses and output electromagnetic power of the compared machines at fixed copper loss value of 30 W is shown in Fig. 9. Consequently, the efficiency characteristic of the investigated machines is depicted in Fig. 10; R-P stands for: rotor-pole. It is obvious that the machine having 10-rotor pole configuration has the largest output power and best efficiency amongst all. The compared machines have relatively low iron loss and negligible eddy current loss values when compared with the output electromagnetic power. The worst performance is seen in the 4-rotor pole topology.

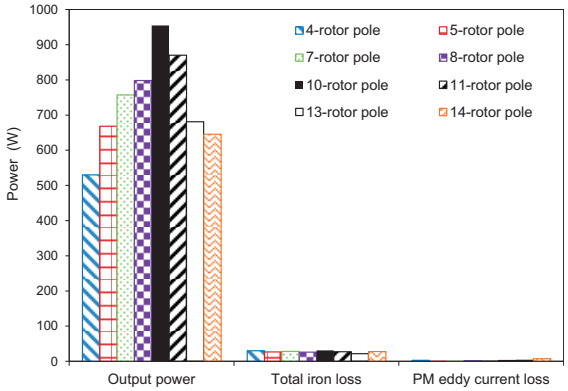

Fig. 9. Comparison of output power and losses topology

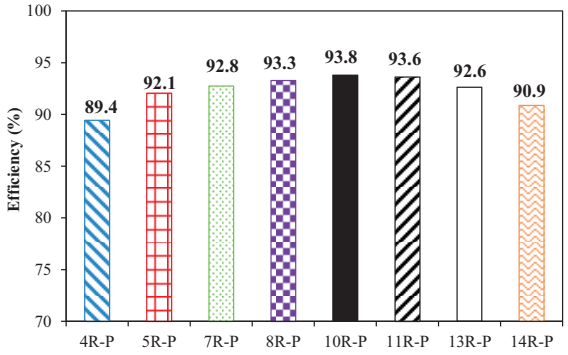

Fig. 10. Comparison of maximum efficiency

4. Test results

Fig. 11 shows the built and tested prototype machine having an 11-rotor pole number, since this particular machine topology produces the largest torque in the whole study. Note that the iron

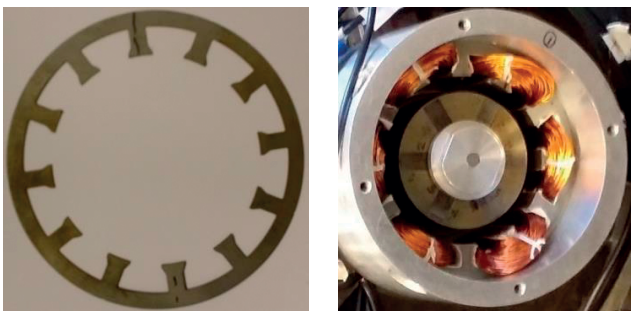

Lamination of outer stator steel Assembled machine

Fig. 11. Tested machine

pieces are held together by a non-magnetic material of 0.5 mm thickness. The manufacturing of the cup-rotor is the most difficult aspect of the fabrication process. It is worth noting that cheap, low carbon, electrical (silicon) laminated steel sheet i.e. steel_1008 is used for both the rotor and stator cores.

The measured back-EMF result with their corresponding spectra is compared with the predicted 3D result in Fig. 12 with an excellent match. It is worth noting that the compared results of Figs. 12 and 13 are based on the exact dimensions of the fabricated machine. Further, the static torque versus the rotor position of the tested machine is compared in Fig. 13 with good agreement. Similarly, the estimated torque ripple, T_{ripple}, from the torque versus the time waveform of the simulated 11-rotor pole machine at nominal current is calculated using (11) and it yielded a ripple value of 8.1%.

$$T_{\text{ripple}} = \frac{\text{Maximum torque} - \text{Minimum torque}}{\text{Average torque}} 100\%. \tag{11}$$

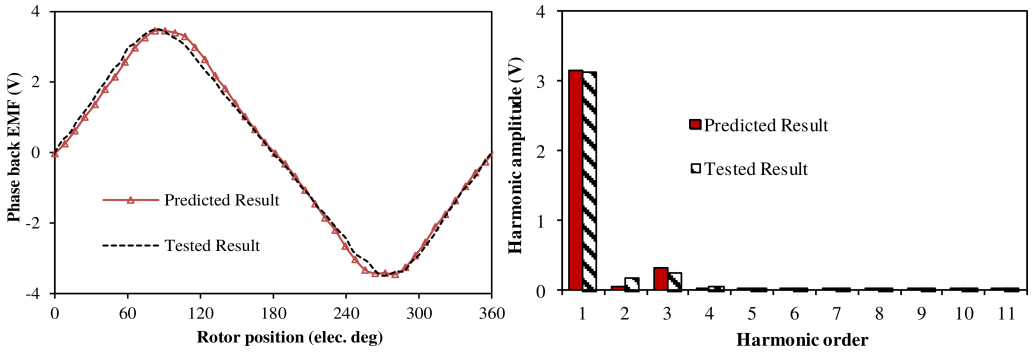

(a) Waveforms (b) Spectra

Fig. 12. Comparison of no-load induced EMF, 400 rpm

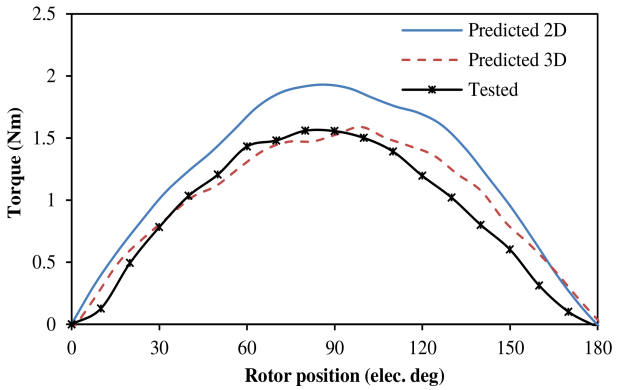

Fig. 13. Static torque versus rotor position, $I_A = 15$ A, $I_B = I_C = -7.5$ A

5. Conclusions

Permanent magnet machines having different winding topologies with two separate stators are presented. The quantitative comparison of the machine having different stator and rotor pole combinations is also given. The analysis shows that, the largest torque-density is observed in the 11-rotor pole and 10-rotor pole machines having alternate- and all-pole-wound configurations, respectively. More so, better sinusoidal EMF waveforms with less ripple effect are obtained in the odd-rotor pole machines, compared to the asymmetric and non-sinusoidal waveforms of most of the even rotor ones. In general, the machines having alternate-pole-windings exhibit larger torque density than their all-pole-wound equivalents. Above all, the tested machine results show excellent agreement.

Acknowledgements

The first author would like to thank The Commonwealth Scholarship Commission, UK for the sponsorship to run a PhD programme at The University of Sheffield, UK, during which period this research was carried out.

References

[1] Li S., Li Y., Sarlioglu B., *Partial irreversible demagnetization assessment of flux-switching permanent magnet machine using ferrite permanent magnet material*, IEEE Transactions on Magnetics, vol. 51, no. 7, p. 8106209 (2015).

[2] Hua W., Zhang G., Cheng M., *Investigation and design of a high-power flux-switching permanent magnet machine for hybrid electric vehicles*, IEEE Transactions on Magnetics, vol. 51, no. 3, p. 8201805 (2015).

[3] Bianchi N., Bolognani S., Pré M.D., Grezzani G., *Design considerations for fractional-slot winding configurations of synchronous machines*, IEEE Transactions on Industry Applications, vol. 42, no. 4, pp. 997–1006 (2006).

[4] Cheng S.P., Hwang C.C., *Design of high-performance spindle motors with single-layer concentrated windings and unequal tooth widths*, IEEE Transactions on Magnetics, vol. 43, no. 2, pp. 802–804 (2007).

[5] Magnussen F., Lendenmann H., *Parasitic effects in PM machines with concentrated windings*, IEEE Transactions Industry Applications, vol. 43, no. 5, pp. 1223–1232 (2007).

[6] El-Refaie A.M., Jahns T.M., *Impact of winding layer number and magnet type on synchronous surface PM machines designed for wide constant-power speed range operation*, *IEEE Transactions on Energy Conversion*, vol. 23, no. 1, pp. 53–60 (2008).

[7] Bianchi N., Bolognani S., Pré M.D., *Impact of stator winding of a five-phase permanent-magnet motor on postfault operations*, IEEE Transactions on Industrial Electronics, vol. 55, no. 5, pp. 1978–1987 (2008).

[8] Wrobel R., Mellor P.H., McNeill N., and Staton D.A., *Thermal performance of an open-slot modular-wound machine with external rotor*, IEEE Transactions on Energy Conversion, vol. 25, no. 2, pp. 403–411 (2010).

[9] Hwang C.C., Chang C.M., Hung S.S., Liu C.T., *Design of high performance flux switching PM machines with concentrated windings*, IEEE Transactions on Magnetics, vol. 50, no. 1, p. 4002404 (2014).

[10] Chen J.T., Zhu Z.Q., *Comparison of all- and alternate-poles-wound flux-switching PM machines having different stator and rotor pole numbers*, IEEE Transactions on Industry Applications, vol. 46, no. 4, pp. 1406–1415 (2010).

[11] Ishak D., Zhu Z.Q., Howe D., *Comparison of PM brushless motors, having either all teeth or alternate teeth wound*, IEEE Transactions on Energy Conversion, vol. 21, no. 1, pp. 95–103 (2006).

[12] Chen J.T., Zhu Z.Q., Iwasaki S., Deodhar R., *Comparison of losses and efficiency in alternate flux-switching permanent magnet machines*, Proceedings of International Conference on Electrical Machines (ICEM), Rome, Italy, pp. 1–6 (2010).

[13] Jian L., Chau K.T., Gong Y., Jiang J.Z., Yu C., Li W., *Comparison of coaxial magnetic gears with different topologies*, IEEE Transactions on Magnetics, vol. 45, no. 10, pp. 4526–4529 (2009).

[14] Wu Y.C., Wang C.W., *Transmitted torque analysis of a magnetic gear mechanism with rectangular magnets*, Applied Mathematics and Information Science, vol. 9, no. 2, pp. 1059–1065 (2015).

[15] Tlali P.M., Gerber S., Wang R.J., *Optimal design of an outer-stator magnetically geared permanent magnet machine*, IEEE Transactions on Magnetics, vol. 52, no. 2, p. 8100610 (2016).

[16] Hua W., Cheng M., Zhu Z.Q., Howe D., *Design of flux-switching permanent magnet machine considering the limitation of inverter and flux-weakening capability*, Proceedings of IEEE Industry Applications Annual Conference Meeting, Tampa, FL, USA, pp. 2403–2410 (2006).

[17] Zhu Z.Q., Chen J.T., *Advanced flux-switching permanent magnet brushless machines*, IEEE Transactions on Magnetics, vol. 46, no. 6, pp. 1447–1453 (2010).